Origin of bursting *p*H oscillations in an enzyme model reaction system

Ronny Straube,[1,*] Dietrich Flockerzi,[2] Stefan C. Müller,[1] and Marcus J. B. Hauser[1,†]
[1]*Abteilung Biophysik, Institut für Experimentelle Physik, Otto-von-Guericke Universität, Universitätsplatz 2, D-39106 Magdeburg, Germany*
[2]*Max-Planck-Institut für Dynamik komplexer technischer Systeme, Sandtorstrasse 1, D-39106 Magdeburg, Germany*
(Received 15 July 2005; published 6 December 2005)

The transition from simple periodic to bursting behavior in a three-dimensional model system of the hemin–hydrogen-peroxide–sulfite *p*H oscillator is investigated. A two-parameter continuation in the flow rate and the hemin decay rate is performed to identify the region of complex dynamics. The bursting oscillations emerge subsequent to a cascade of period-doubling bifurcations and the formation of a chaotic attractor in parameter space where they are found to be organized in periodic-chaotic progressions. This suggests that the bursting oscillations are not associated with phase-locked states on a two-torus. The bursting behavior is classified by a bifurcation analysis using the intrinsic slow-fast structure of the dynamics. In particular, we find a slowly varying quasispecies (i.e., a linear combination of two species) which acts as an "internal" or quasistatic bifurcation parameter for the remaining two-dimensional subsystem. A systematic two-parameter continuation in the internal parameter and one of the external bifurcation parameters reveals a transition in the bursting mechanism from sub-Hopf/fold-cycle to fold/sub-Hopf type. In addition, the slow-fast analysis provides an explanation for the origin of quasiperiodic behavior in the hemin system, even though the underlying mechanism might be of more general importance.

DOI: 10.1103/PhysRevE.72.066205 PACS number(s): 82.40.Bj, 82.40.Qt, 82.20.Wt

I. INTRODUCTION

Complex oscillatory patterns in chemical and biological systems have been the focus of scientific interest for several decades. Mixed-mode and bursting oscillations are of particular interest due to their potential relevance for signal transduction processes in biological systems. While mixed-mode oscillations (MMO's) were first observed in chemical reactions such as the Belousov-Zhabotinsky (BZ) [1,2] and later the peroxidase-oxidase (PO) reaction system [3–5], bursting behavior was predominantly reported for biological processes such as nerve signal conduction [6,7], signal transduction dynamics in the cell involving calcium ions as second messengers [8,9], and the secretion of insulin by pancreatic β-cells [10–12].

However, the distinction between mixed-mode and bursting oscillations is somewhat arbitrary and seems to reflect the context in which they were found experimentally. Both types of dynamics can be characterized as a repeating pattern of L large amplitude oscillations followed by S small ones. The corresponding dynamical states are denoted as L^S, a nomenclature that has particularly prevailed for MMO's. Alternatively, bursting behavior can be conveniently classified by a slow-fast analysis following Rinzel and Ermentrout [13]. Systems exhibiting bursting oscillations typically involve a fast oscillatory subsystem which is coupled to a slowly evolving variable acting as a quasistatic bifurcation parameter for the fast subsystem. Accordingly, the bursting behavior can be classified by the type of bifurcations occurring in the fast subsystem that lead to the emergence and disappearance of the bursting state [14]. It is noteworthy that, although the article by Rinzel and Ermentrout [13] can be regarded as the seminal work in which this kind of slow-fast analysis was systematically introduced, there exist earlier papers applying basically this technique: An example is the work by Showalter and colleagues [15] on the so-called reversible Oregonator model for the BZ reaction which already contains first attempts towards a slow-fast analysis to understand the origin of bursting oscillations in their model.

Mixed-mode and bursting oscillations are frequently encountered in the transition region from simple periodic or quasiperiodic to chaotic behavior. It was found experimentally that in the BZ [2] as well as in the PO system [5] the MMO's are organized in Farey sequences similar to the periodic states that emerge along the "quasiperiodic route to chaos" on an invariant two-torus. Numerical simulations of the corresponding model systems supported these results [4,16–18]. However, Hauser and Olsen [3] found MMO's in the PO system which were associated with a saddle-focus homoclinic orbit instead of a two-torus. Similarly, Koper [19] observed MMO's in a three-variable extension of the Boissonade-DeKepper model [20] which emerge from a neutrally twisted homoclinic orbit in a codimension-2 bifurcation. Another possible scenario was put forward by Ringland and colleagues [21], who showed that a family of two-extremum maps may (in a certain limit) equally account for the ordering of MMO's into Farey sequences without the necessity of involving a two-torus. Goryachev and coworkers [22] found a concrete realization of this map in terms of a Poincaré map associated with the three-dimensional flow of another three-variable extension of the Boissonade-DeKepper model which accounts for a qualitative description of transient MMO's in the BZ reaction. They

*Present address: Hahn-Meitner-Institut Berlin, Glienicker Str. 100, D-14109 Berlin, Germany.
†Corresponding author. Electronic address: marcus.hauser@physik.uni-magdeburg.de

TABLE I. Rate constants and inflow stream concentrations for the hemin *p*H oscillator.

$k_1=0.2\ \mathrm{M^{-1}\ s^{-1}}$	$k_2=1.5\ \mathrm{M^{-1}\ s^{-1}}$	$k_3=8.5\times10^6\ \mathrm{M^{-2}\ s^{-1}}$	$k_4=1000\ \mathrm{s^{-1}}$
$k_5=10^{10}\ \mathrm{M^{-1}\ s^{-1}}$	$k_6=0.011\ \mathrm{s^{-1}}$	$k_7=2.5\times10^4\ \mathrm{M^{-1}\ s^{-1}}$	$k_8=2.5\times10^{-4}\ \mathrm{s^{-1}}$
$x_1^0=0.025\ \mathrm{M}$	$x_2^0=0.045\ \mathrm{M}$	$x_4^0=2.2\times10^{-4}\ \mathrm{M}$	$x_5^0=3\times10^{-4}\ \mathrm{M}$

reported that the MMO's are embedded into a horseshoe-type attractor.

In the present article, we investigate the bursting oscillations in the hemin–hydrogen-peroxide–sulfite system [23–25] which belongs to the class of so-called *p*H oscillators. These systems exhibit an autocatalytic production of H^+ ions while they differ in the species that provides for a negative feedback to allow for oscillatory dynamics. In earlier studies, inorganic compounds such as hexacyanoferrate [26,27], thiosulfate [28], sulfide [29], or hydrogen carbonate [30] have been used to accomplish the negative feedback. The corresponding experimental and numerical investigations revealed that *p*H oscillators may support a period-doubling route to chaos [27] as well as complex oscillatory patterns such as bursting oscillations [28,31]. However, a detailed bifurcation analysis unveiling the nature of the complex oscillatory patterns in *p*H oscillator systems has, to our knowledge, not yet been performed. This task is the main objective of the present article. In particular, we are interested in the elucidation of the underlying bursting mechanism and the bifurcations involved in the transition from simple periodic to bursting oscillations.

A. Hemin–hydrogen-peroxide–sulfite system

The basis for our analysis is the reaction mechanism of the hemin–hydrogen-peroxide–sulfite system as it was proposed in [25]. Similar to other *p*H oscillators, it involves an autocatalytic production of H^+ while the negative feedback, preventing an unbounded production of H^+, is provided by reactions involving hemin, a biocompatible mimic for heme-containing enzymes. Assuming mass-action kinetics, the most prominent dynamical features of the hemin system such as bursting or mixed-mode oscillations were described by a six-dimensional system of ordinary differential equations (ODE system) in a previous study [25]. Using the method of quasi-integrals, a three-dimensional approximation to the six-dimensional system was derived by a slow manifold reduction while retaining the local bifurcation structure [32]. The three-dimensional system reads

$$\begin{aligned}
\dot{x} &= k_0 x_2^0 - x(k_0 + k_1 s(x,y) + \{k_2 + k_3[a - x - y + s(x,y)]\}) \\
&\quad \times [x_1^0 - x_2^0 + x - s(x,y)], \\
\dot{y} &= -k_0 y - k_6 y + k_7 z[a - x - y + s(x,y)], \\
\dot{z} &= k_0(x_5^0 - z) - k_8 z + k_6 y - k_7 z[a - x - y + s(x,y)], \qquad (1)
\end{aligned}$$

where $s(x,y)$ stands for the slow manifold of the six-dimensional system given by

$$s = \frac{1}{2}\left(x + y - a - \frac{k_4}{k_5}\right) + \frac{1}{2}\sqrt{\left(x + y - a + \frac{k_4}{k_5}\right)^2 + 4\frac{k_4}{k_5}(x_4^0 - y)}. \qquad (2)$$

For convenience, we have changed the notation of the variables from (y_1, y_2, y_3, y_4) (which were used in [32]) to (x,y,z,s). The numerical values of the rate constants $k_1, \ldots, k_8$ and the concentrations x_i^0 in the inflow streams of a continuous-flow stirred tank reactor are compiled in Table I; a is an abbreviation for $x_4^0 - x_1^0 + x_2^0$. k_0 denotes the flow rate through the reactor. According to the experimental situation, it is used as the principal bifurcation parameter for the ODE system (1) ranging in the interval $k_0 \in [1\times10^{-4}\ \mathrm{s^{-1}}, 4.5\times10^{-4}\ \mathrm{s^{-1}}]$.

Next, we perform the linear coordinate transformation

$$p = y + z, \qquad (3)$$

which is motivated by the following two observations: First, after the transformation (3) one of the equations in (1) becomes affine and more simple:

$$\begin{aligned}
\dot{x} &= k_0 x_2^0 - x(k_0 + k_1 s(x,y) + \{k_2 + k_3[a - x - y + s(x,y)]\}) \\
&\quad \times [x_1^0 - x_2^0 + x - s(x,y)], \\
\dot{y} &= -(k_6 + k_0) y + k_7 (p - y)[a - x - y + s(x,y)], \\
\dot{p} &= k_0(x_5^0 - p) - k_8(p - y). \qquad (4)
\end{aligned}$$

Second, in chemical terms, p corresponds to the total concentration of hemin species in the system which turns out to evolve on a slower time scale than the x-y subsystem. Note that the slow manifold $s(x,y)$ is independent of p. Later on, the ODE system (4) will be the starting point for a slow-fast analysis where the slow variable p is used as a quasistatic bifurcation parameter for the dynamics in the transversal x-y subsystem.

As can be grasped from the third equation of (4), the slow dynamics of the p variable is basically determined by the flow rate k_0 and the rate constant k_8 which represents the decay rate of the hemin species. Since the experimental value of k_8 has not been precisely determined so far, we shall use it, in addition to the flow rate k_0, as a second bifurcation parameter. The mechanistic role of hemin is to prevent the unbounded production of H^+ species and, thus, the hemin decay rate should be a sensible parameter. In fact, if k_8 is identically zero, the ODE systems (1) and (4) become essentially two dimensional and no complex dynamics is possible anymore.

B. Outline

In the next section, we introduce the software packages and scalings of the variables used in the numerical investigations. In Sec. III, the most important dynamical features of the ODE system (1) [or equivalently (4)] are summarized and presented in a two-parameter bifurcation diagram using the flow rate k_0 and the decay rate of hemin k_8 as parameters. We show that the simple periodic oscillations either appear via a supercritical or by a subcritical Hopf bifurcation, depending on the value of the hemin decay rate. In the subcritical case, stable oscillations are also found. However, they emerge in a more complex scenario involving a saddle-node bifurcation of periodic orbits and a subsequent Neimark-Sacker bifurcation. The transition from simple periodic to bursting oscillations is found to occur along a branch of period doubling bifurcations in the two-parameter plane spanned by k_0 and k_8.

In Sec. IV, we perform a slow-fast analysis of the ODE system (4) in order to study the dynamical origin of the bursting oscillations. To this purpose, the total concentration of hemin species p is used as an "internal" or quasistatic bifurcation parameter for the fast x-y subsystem. As a result, we obtain a certain bifurcation scenario in the fast subsystem for each fixed value of the flow rate k_0 which acts as an "external" bifurcation parameter in the system. Since the attracting states in the fast subsystem, in general, depend on the current value of k_0, we perform a two-parameter continuation using the internal bifurcation parameter p together with the flow rate k_0 as the second parameter to monitor the deformation of the invariant sets in the two-dimensional fast subsystem. This analysis reveals an interesting transition in the bursting behavior from sub-Hopf/fold-cycle to fold/sub-Hopf type according to the classification scheme proposed by Izhikevich [14].

In Sec. V, we summarize our results and discuss the origin of quasiperiodic behavior in the hemin system in terms of the invariant sets of the fast subsystem.

II. METHODS

The numerical simulations were performed with the freely available software package XPPAUT [34]. Due to the stiffness of the ODE systems (1) and (4), the "STIFF" integrator [34,35] with a tolerance of 10^{-5} was chosen to ensure numerical stability. For the calculation of one- and two-parameter bifurcation diagrams, we used a version of AUTO that is integrated in the XPPAUT environment, as well as two other freely available continuation packages: CONTENT [36] and MATCONT [37]. The advantage of the latter packages is their ability to detect codimension-2 bifurcation points by taking into account the analytical expressions for the derivatives of the vector field up to fourth order. We also made use of their capability to calculate normal form coefficients of several codimension-2 bifurcations as well as eigenvalues and multipliers along branches of stationary and oscillatory solutions.

As they stand, the variables x, y, z, and p of the ODE systems (1) and (4) still possess dimensions and vary in magnitude between 10^{-4} and 10^{-2} mol l^{-1}. For convenience, we rescaled these variables according to

$$x' = 10^2 \text{ mol}^{-1}\, l\, x,$$

$$y' = 10^4 \text{ mol}^{-1}\, l\, y,$$

$$z' = 10^4 \text{ mol}^{-1}\, l\, z, \tag{5}$$

where the primed variables denote the dimensionless quantities used in the simulations and in the figures. For convenience, we shall henceforth drop the prime again. The scaling ensures that the maximum of the variables during their temporal evolution is of order unity.

The two principal bifurcation parameters in our system are the flow rate k_0 and the decay rate k_8 of hemin which are both simple rate constants having the dimension s^{-1}. Their order of magnitude is 10^{-4}. Thus, whenever we present numerical values of any of the two parameters, they are to be understood in units of 10^{-4} s^{-1}. For example, in the ODE system (1), we found a subcritical Hopf bifurcation at $(k_0,k_8)=(1.6461\times10^{-4}\ s^{-1}, 2.5\times10^{-4}\ s^{-1})$ which due to our convention would simply be denoted as $(k_0,k_8)=(1.6461,2.5)$.

III. DYNAMICS AND LOCAL BIFURCATIONS

The local bifurcation diagram for the three-dimensional ODE system (1) was found to be in very good quantitative agreement with that of the original six-dimensional system [25,32]. However, the nature of the transition from simple periodic oscillations to more complex oscillatory patterns has not yet been resolved. Therefore, we perform a two-parameter continuation to gain some insight into the global bifurcation structure of the ODE system (1) [and equally (4)].

A. Two-parameter continuation in k_0 and k_8

Figure 1 shows the two-parameter bifurcation diagram for the ODE system (1) where the flow rate k_0 and the hemin decay rate k_8 have been used as continuation parameters. It basically consists of five regions: In regions 1 and 5, there is only one stable stationary state. Coming from region 1, the stationary state loses stability via a subcritical Hopf (SH_1, dashed line) or a supercritical Hopf (H, solid line) bifurcation. In the latter case this leads immediately to the emergence of stable oscillations which remain of simple periodicity throughout region 2 while in the former case simple periodic oscillations also arise, but through a series of secondary bifurcations that will be discussed below. The two branches of Hopf bifurcations meet in a codimension-2 bifurcation point, the generalized Hopf bifurcation GH_1 at $k_8=1.8920$, where the first Liapunov coefficient vanishes (cf. [33]).

Upon following the curve of supercritical Hopf bifurcations (H) towards lower values of k_8, the curve again becomes subcritical (SH_2) at a second generalized Hopf bifurcation (GH_2) where k_8 is negative. Note that the region where k_8 is negative does not have a physical significance in

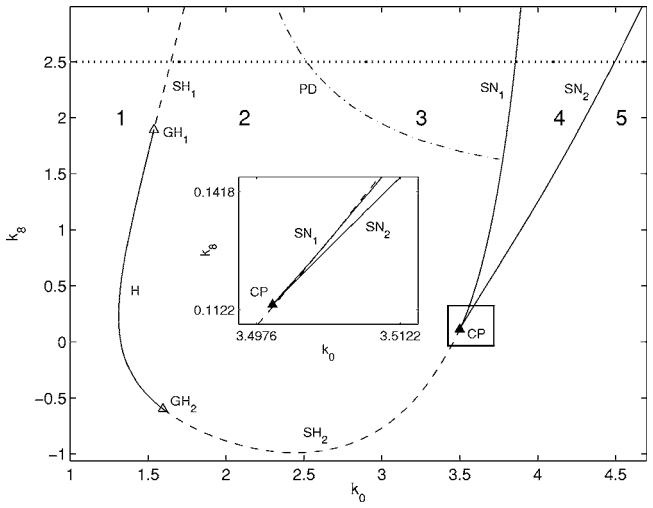

FIG. 1. Two-parameter bifurcation diagram in the flow rate k_0 and the hemin decay rate k_8. Bursting oscillations are stable in region 3, which is bounded by the period-doubling curve (PD) and the saddle-node curve SN_1. The dotted line at $k_8=2.5$ marks the parameter path along which the codimension-1 bifurcation diagram in Fig. 2 has been calculated. Symbols denote SH_i, curves of subcritical Hopf bifurcations (dashed line); H, curve of supercritical Hopf bifurcations (solid line); SN_i, curves of saddle-node bifurcations of fixed points (solid line); PD, curve of period-doubling bifurcations (dash-dotted line); codimension-2 points: GH_i, generalized Hopf bifurcations (open triangle); CP, cusp (solid triangle; see also the inset).

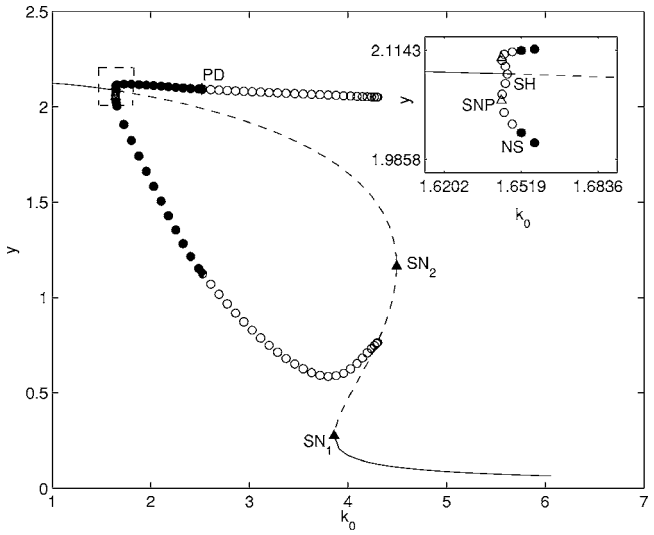

FIG. 2. One-parameter bifurcation diagram along the line $k_8=2.5$ (cf. Fig. 1). Simple periodic oscillations (solid circles) emerge via a subcritical Hopf bifurcation (inset, SH) followed by a saddle-node bifurcation of periodic orbits (inset, open triangle, SNP) and an (inverse) Neimark-Sacker bifurcation (inset, solid square, NS). Between SNP and SH, the only stable attractor is a fixed point, while a torus is stable between SH and NS. Mixed-mode oscillations are observed beyond the period-doubling (PD) bifurcations where the primary limit cycle (open circles) is unstable (see text for details). The oscillatory region extends up to the saddle-node bifurcation SN_1, where a homoclinic bifurcation occurs (see also Fig. 6). For the oscillatory states, the minimum and maximum amplitudes of the oscillation are plotted.

our model; it is merely included for a consistent description of the bifurcation scenario. Finally, the subcritical Hopf bifurcation curve turns into a curve of neutral saddles (where the eigenvalues fulfill $\lambda_1+\lambda_2=0$ with $\lambda_1, \lambda_2 \in \mathbb{R}$) close to the cusp singularity (CP, solid triangle). However, these neutral saddles do not correspond to a bifurcation. The region in the vicinity of the cusp point is magnified in the inset of Fig. 1, which shows that two branches of saddle-node points (SN_1 and SN_2) emanate from CP. The transition from Hopf bifurcations to neutral saddles in conjunction with the two curves of saddle-node bifurcations is reminiscent of a Bogdanov-Takens point although such a point has not been detected.

Bursting oscillations are stable in region 3, which is bounded by a curve of period-doubling bifurcations (PD) and the left branch of the saddle-node points SN_1. In region 4 two saddle points coexist with one stable equilibrium, which remains the only fixed point in region 5 where it is stable. Accordingly, all trajectories settle down to a stationary state in regions 4 and 5.

The partition into five regions, however, only gives a first impression of the expected dynamics of the ODE system (1). For example, there is a narrow band to the right of the period-doubling curve PD where an entire cascade of period-doubling bifurcations occurs as the flow rate k_0 is increased for a fixed value of k_8. Subsequently, a folded chaotic attractor emerges before the first periodic bursting oscillations appear in region 3. Furthermore, it is known from the normal form theory of codimension-2 bifurcations [33] that there is an additional curve bifurcating from the generalized Hopf point GH_1 in Fig. 1 (in our case towards higher values of k_8) along which a saddle-node bifurcation of periodic orbits (SNP) takes place (not shown). A similar curve also bifurcates from the second generalized Hopf point GH_2.

B. Bifurcations along a one-parameter path

In order to obtain a full picture of the bifurcation sequences, we take a section along the one-parameter path $k_8=2.5$ in the k_0-k_8 plane (dotted line, Fig. 1) where the stationary state disappears by a subcritical Hopf bifurcation and simple periodic oscillations arise in the following scenario (Fig. 2, inset): The stable stationary state (solid line) loses stability at $k_0=1.6461$ via a subcritical Hopf bifurcation (SH) giving rise to an unstable limit cycle with one unstable dimension (one Floquet multiplier outside the unit circle). It is followed by a saddle-node bifurcation of periodic orbits (SNP) at $k_0=1.6438$ where the second multiplier also leaves the unit circle and the limit cycle gains a second unstable dimension. In the narrow parameter interval between the SNP and SH bifurcation points, the stationary state is the only attractor since the coexisting limit cycle is unstable. Stable oscillations, however, arise at $k_0=1.6519$ by an (inverse) Neimark-Sacker (NS) bifurcation where both multipliers simultaneously cross the unit circle inwards. Thus, there is a stable two-torus bifurcating to the left of the Neimark-Sacker point (towards lower k_0 values) where it coexists with the saddle-point (corresponding to the dashed line in the inset of Fig. 2) in the parameter interval k_0

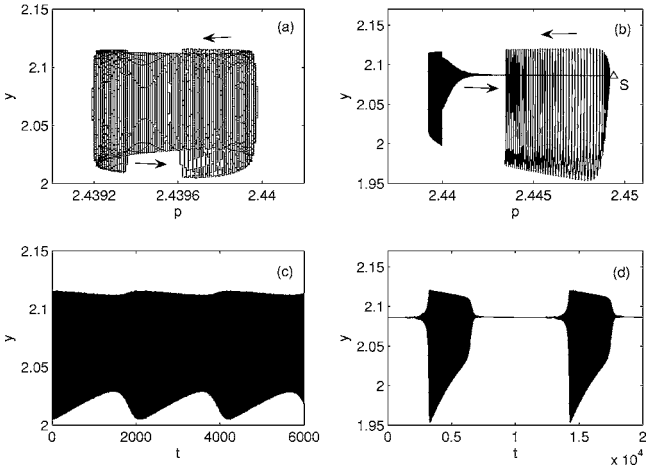

FIG. 3. Deformation of the two-torus as the flow rate k_0 is decreased from $k_0=1.65189$ (a),(c) to $k_0=1.6518$ (b),(d): (a),(b) represent projections onto the p-y plane while (c),(d) depict the corresponding time series. Close to the Neimark-Sacker point NS in the inset of Fig. 2, the torus looks smooth (a). At a slightly decreased value of the flow rate, the "inner part" of the torus rapidly shrinks to a linelike manifold along which the trajectory approaches the stable manifold of the saddle point S (b).

$\in (1.6461, 1.6519)$,i.e., up to the subcritical Hopf bifurcation SH.

Before proceeding with the discussion of the bifurcations along the one-parameter path $k_8=2.5$, we shall describe the phase flow on the torus in more detail.

1. Two-torus with unusual phase flow

In Fig. 3 we monitor the deformation of the torus as the flow rate k_0 is decreased. In the projections on the p-y plane [Figs. 3(a) and 3(b)], we stopped the numerical integration before the trajectory made a full revolution on the torus to reveal a portion of the flow along the "inner part" of the torus. A sharp transition from a smooth torus shown in Fig. 3(a) at $k_0=1.651\,89$ close to the NS bifurcation point to a highly distorted one at $k_0=1.651\,80$ [Fig. 3(b)] is observed. The arrows indicate the direction of the phase flow along the torus.

The reason for the rather unusual phase flow is the following: Imagine a two-torus as a direct product of two circles; then, the angular velocity along the circle with the larger radius is much higher than that along the circle with the smaller radius. This behavior is opposite to the usual situation. In other words, the unusual phase flow is a result of the time-scale separation in the ODE system (4) where the trajectory moves much faster in the x-y directions than along the p direction.

The saddle point S (corresponding to the dashed line in the inset of Fig. 2) that emerges subsequent to the subcritical Hopf bifurcation SH in Fig. 2 acts as an organizing center for the torus as can be seen in Fig. 3(b): The flow on the torus moves along the two-dimensional unstable manifold of the saddle point to approach the "outer part" of the torus. Then it moves to the left (i.e., towards lower p values) until it changes direction and returns along the one-dimensional stable manifold of the saddle. The reason for the trajectory to change its direction can be grasped from the slow-fast analysis of (4) and will be discussed in Sec. V.

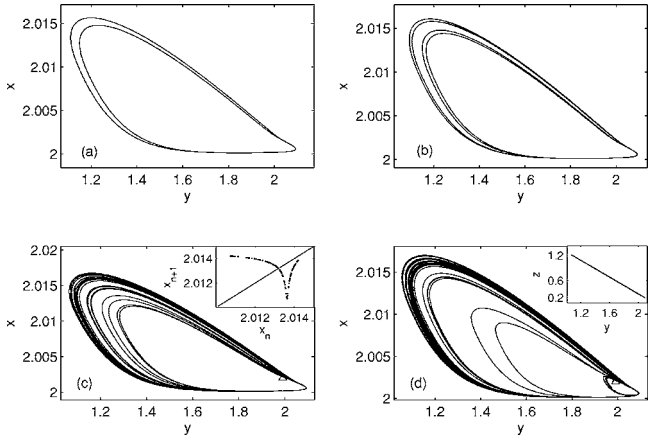

FIG. 4. Bifurcation scenario beyond the period-doubling bifurcation PD in Fig. 2: period-2 (a) at $k_0=2.52$, period-4 (b) at $k_0=2.5252$, and two subsequent chaotic orbits (c),(d) at $k_0=2.529$ and $k_0=2.53$, respectively, are shown. The chaotic trajectory in (c) performs only large amplitude oscillations while that one in (d) makes irregular excursions to the neighborhood of the saddle point (open triangle). The associated Poincaré map of the chaotic orbit in (c) is shown in the inset. It exhibits the shape of an inverse tent map with a cuspoid tip (see text for details). The inset in (d) shows the same chaotic orbit as in (d) but in a y-z projection where it becomes apparent that the chaotic attractor is contained in a thin layer in phase space.

As the flow rate k_0 is further decreased, the overall shape of the torus in Fig. 3(b) does not change significantly anymore. However, the time spent by the trajectory along the stable manifold of the saddle point S gradually increases until the torus and saddle point have eventually disappeared to the left of the subcritical Hopf point (SH) where only a stable stationary point exists (cf. inset Fig. 2).

2. Period-doubling route to chaos

We continue the discussion of the codimension-1 bifurcation diagram shown in Fig. 2 where k_8 is fixed at 2.5. The simple periodic oscillations (solid circles) were generated by a Neimark-Sacker bifurcation at $k_0=1.6519$. They remain stable up to $k_0=2.5169$ where the first of a series of period-doubling (PD) bifurcations renders the simple oscillations unstable and creates a stable period-2 cycle [Fig. 4(a)]. The next two period-doubling bifurcations were resolved at $k_0=2.5241$ [Fig. 4(b)] and 2.5253 (not shown).

During the period-doubling cascade, the two multipliers of the primary unstable limit cycle (open circles in Fig. 2) rapidly diverge until they are separated by approximately 12 orders of magnitude—i.e., $\mu_1 \sim 10^6$ and $\mu_2 \sim 10^{-6}$. Thus, the associated Poincaré map exhibits a strong contraction in one and a fast expansion in the other direction, indicating the creation of a folded attractor for the subsequent chaotic regime. In Fig. 4(c) we show a chaotic trajectory together with its Poincaré map (cf. inset) at $k_0=2.529$. For the Poincaré map, we plot the value of the x variable each time the y

variable passes a local minimum against the value of x at the preceding minimum of y. As a result, we obtain a Poincaré map exhibiting a typical (asymmetric) tent-map shape indicating chaotic behavior. Indeed, the characteristic Liapunov exponent, which is a measure for the local divergence of initially close trajectories, is found to be 0.84 at $k_0=2.529$. Figure 4(d) shows a nearby chaotic orbit at $k_0=2.530$ with a characteristic Liapunov exponent of 1.12. This orbit differs from the former one in that the trajectory now also performs small amplitude excursions to the neighborhood of the saddle point (open triangle) in an irregular fashion, indicating the upcoming bursting oscillations. The inset in Fig. 4(d) shows the same chaotic trajectory at $k_0=2.53$ but in a y-z projection where it becomes obvious that y and z are basically anticorrelated which causes the chaotic attractor to be contained in a thin layer in phase space, a property that also holds for the subsequent bursting oscillations. Due to the anticorrelation between y and z, their sum $y+z$ changes only slowly in time, which again suggests introducing the sum of y and z as a new variable according to (3).

3. Bursting oscillations

Subsequent to the formation of the chaotic attractor, we observe periodic-chaotic progressions of bursting oscillations (or MMO's) which are organized into Farey sequences as described below. Notice that the bursting states are not shown in the one-parameter bifurcation diagram of Fig. 2 since they do not bifurcate from the primary periodic orbit. Instead, they emerge as periodic windows interspersing the chaotic regime that follows the period-doubling bifurcation PD. This suggests that they belong to isolated bifurcation curves. Therefore, we present some of the bursting states that were found by direct numerical integration at the corresponding parameter values.

The first periodic bursting state along the one-parameter path at $k_8=2.5$ (cf. Fig. 2) is observed at $k_0=2.545$ where 11 large amplitude oscillations alternate with 20 small excursions (Fig. 5). According to the mixed-mode nomenclature (L^S), this state is denoted as 11^{20}. Figure 5(a) shows a projection onto the x-y plane (similar to that in Fig. 4). However, if we regard the same state in the p-y projection [Fig. 5(b)], the "unfolding" of the bursting oscillations along the p direction becomes apparent: In the x-y projection [Fig. 5(a)] the small amplitude oscillations are located in the lower right corner while in Fig. 5(b) they occur along a linelike manifold at $y\sim 2.1$. In Fig. 5(c) we present the time series corresponding to the phase portraits of Figs. 5(a) and 5(b). The dashed rectangular region is magnified in Fig. 5(d) showing the small amplitude oscillations.

As the flow rate k_0 increases from 2.545, where a 11^{20} state is observed, to $k_0=3.778$, narrow chaotic windows alternate with further periodic windows which contain bursting states with a gradually decreasing number L of large amplitude oscillations. This periodic-chaotic sequence approaches the window corresponding to $L=1$ at $k_0=3.235$ where a 1^{13} state is stable. Within each periodic window of fixed L, we find Farey sequences of bursting states with a different number S of small amplitude oscillations. For example, in the periodic window corresponding to the 4^S states, the following progression was numerically resolved: 4^{17} ($k_0=2.768$) $\rightarrow 4^{18}$ ($k_0=2.780$) $\rightarrow 4^{19}$ ($k_0=2.800$) $\rightarrow 4^{20}$ ($k_0=2.830$). In the transition region between two states L^S and L^{S+1}, narrow chaotic windows as well as concatenated states of the form L^SL^{S+1} are found. The latter ones are periodic patterns that repeat after two revolutions of the trajectory while their number of small amplitude oscillations differs by one. For the example above, the $4^{17}4^{18}$ state is found at $k_0=2.775$ while the other two states, $4^{18}4^{19}$ and $4^{19}4^{20}$, occur at $k_0=2.795$ and 2.817, respectively.

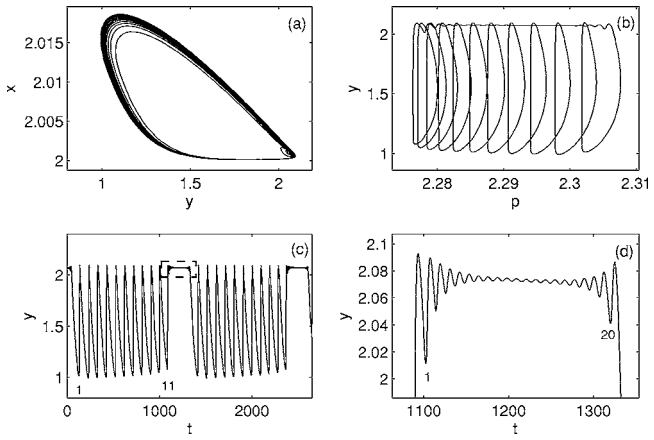

FIG. 5. The 11^{20} MMO at $k_0=2.545$ is shown in a y-x projection (a) and in a p-y projection (b) from which the unfolding of the mixed-mode state along the p direction becomes apparent. The corresponding time series is presented in (c) while the dashed rectangular region in (c) is magnified in (d) showing the small amplitude oscillations.

The parameter window, where L^S states are stable, becomes larger as L gets smaller. At $k_0=3.390$, the number of small amplitude oscillations for the 1^S progression already exceeds 20, but their amplitudes are too small to be counted. As the sequence of 1^S states approaches $k_0=3.778$, the number of small amplitude oscillations steadily increases while the chaotic region between two such states becomes broader. Thus, one may suspect that within each periodic window of a fixed number of large amplitude oscillations, L^S states with arbitrary integer number S exist though most of them occur in too narrow parameter intervals to be observed in numerical simulations.

Subsequent to the periodic-chaotic progression of bursting oscillations, there is a further parameter interval where we observe simple periodic oscillations which are now of relaxational type and have long periods [Fig. 6(a)]. In Sec. IV we shall show that the hemin system undergoes a transition in the bursting mechanism at $k_0=3.778$ which causes the relaxational character of the oscillations beyond the periodic-chaotic progression of bursting states. The relaxational oscillations terminate at $k_0=3.858$ via a saddle-node homoclinic bifurcation where the saddle-node bifurcation SN_1 (cf. Figs. 1 and 2) occurs on the formerly periodic solution [Fig. 6(b)].

This completes the discussion of the bifurcation diagram Fig. 2 along the one-parameter path at $k_8=2.5$ in Fig. 1.

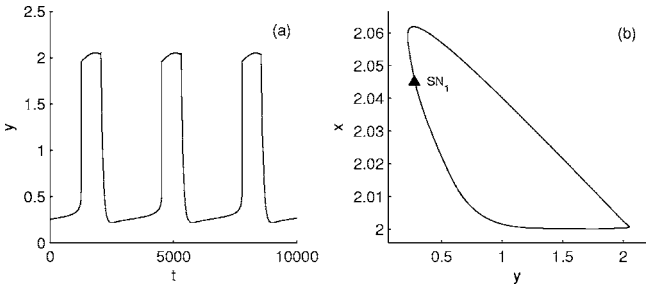

FIG. 6. Large relaxational oscillations at $k_0=3.8$ close to a homoclinic orbit (a). The corresponding trajectory in phase space is shown in (b). SN_1 marks the location where a saddle-node bifurcation will occur at $k_0=3.858$ on the formerly periodic solution. This yields a saddle-node homoclinic bifurcation and causes the oscillations to cease.

IV. GEOMETRICAL DESCRIPTION OF THE BURSTING OSCILLATIONS

In this section we exploit the intrinsic slow-fast structure of the hemin system (4) using the (x,y,p) coordinate system in order to investigate the bursting mechanism directly in phase space. As already mentioned, p evolves on a slower time scale than the transversal x-y subsystem. In particular, the bursting oscillations "unfold" along the p direction [cf. Fig. 5(b)], making the hemin system in the (x,y,p) coordinates particularly suitable for a slow-fast analysis.

The slow-fast analysis is performed by treating the slow variable p as a (quasistatic) bifurcation parameter for the two-dimensional fast subsystem:

$$\dot{x} = k_0 x_2^0 - x(k_0 + k_1 s(x,y) + \{k_2 + k_3[a - x - y + s(x,y)]\}) \times [x_1^0 - x_2^0 + x - s(x,y)],$$

$$\dot{y} = -(k_6 + k_0)y + k_7(p - y)[a - x - y + s(x,y)], \qquad (6)$$

which is simply obtained by omitting the linear equation describing the slow p dynamics,

$$\dot{p} = -(k_0 + k_8)p - k_8 y + k_0 x_5^0, \qquad (7)$$

from the three-dimensional ODE system (4).

The bifurcation structure of Eqs. (6) will be analyzed in two steps: In Sec. IV A we fix the flow rate k_0 at an arbitrarily chosen value and describe the bifurcations in the fast subsystem leading to the bursting oscillations at this particular value of k_0. Depending on the current value of the slow variable p, we will find several stationary and/or oscillatory states in the fast subsystem. These states extend to quasistationary manifolds along the p direction. In particular, fixed points of the fast subsystem extend to linelike quasistationary manifolds while oscillatory states of the fast subsystem become cylinderlike quasistationary manifolds. Due to the finite time scale separation between the fast subsystem and the slow p dynamics, the trajectories of the full three-dimensional system (4) will be confined to the neighborhood of these quasistationary manifolds in phase space.

In a second step, we investigate in Sec. IV B how the quasistationary manifolds, which exist at a particular value of k_0, change in dependence on k_0. Thus, k_0 may be regarded as an external bifurcation parameter for the two-dimensional subsystem (6). In contrast to k_0, the actual value of the slow variable p can not be prescribed. Instead, it evolves dynamically, although within a narrow range of values, according to Eq. (7) and, thus, we have called p an internal bifurcation parameter.

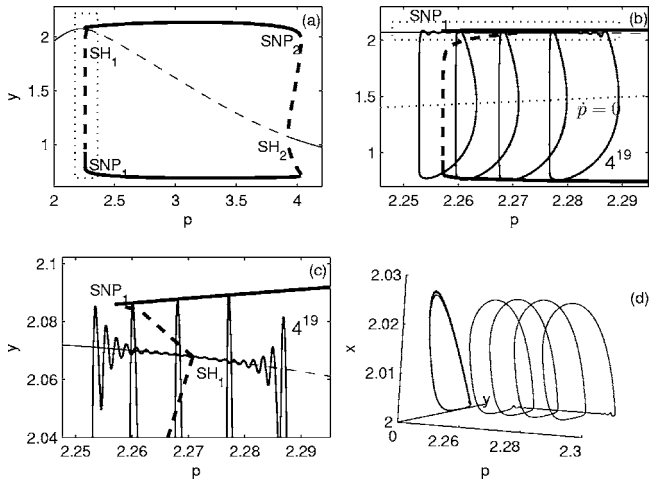

FIG. 7. Slow-fast analysis at a fixed value of the flow rate $k_0=2.8$: The bifurcation diagram of the fast subsystem (6) is shown in (a). The dotted rectangular region is magnified in (b) together with the trajectory (medium solid line) of a 4^{19} state at $k_8=2.5$. The orbit wraps 4 times around the cylinderlike quasistationary manifold that is composed of stable limit cycle solutions and subsequently performs 19 small amplitude oscillations along the linelike quasistationary manifold which is magnified in (c). In (d) a three-dimensional view of the 4^{19} state is shown together with a projection onto the x-y plane. Solid and dashed bold lines denote maxima and minima of a stable and an unstable limit cycle while solid and dashed lines denote stable and unstable fixed points of the fast subsystem.

Note that the truncated ODE system (6) no longer depends on the hemin decay rate k_8, which has been used as a second bifurcation parameter in the two-parameter bifurcation diagram of Fig. 1. Thus, for each fixed value of the external bifurcation parameter k_0, we obtain a set of quasistationary manifolds in the three-dimensional system that exist independently of k_8. However, k_8 determines (together with k_0) the slow dynamics of the p variable according to Eq. (7) and, consequently, it affects the dynamics of the trajectories of the full three-dimensional system.

A. Slow-fast analysis at a fixed value of k_0

In Fig. 7(a) we present the codimension-1 bifurcation diagram for the fast subsystem (6) using p as a bifurcation parameter while k_0 is fixed (arbitrarily) at $k_0=2.8$. Stationary states are plotted as thin lines while the maxima and minima of the oscillatory states are plotted as bold lines. The stability of the states is indicated by using solid lines for stable states and dashed lines for unstable ones. There are two branches of stable stationary states in the fast subsystem: one at $y \sim 2$ and the other at $y \sim 1$. Both of these branches become unstable via subcritical Hopf bifurcations (SH_1 and SH_2)

while the stable oscillations emerge by saddle-node bifurcations (SNP_1 and SNP_2) where a stable limit cycle merges with an unstable one.

The magnification of the dotted rectangular region of the bifucation diagram in Fig. 7(a) is displayed in Fig. 7(b). It shows the bifurcations in the fast subsystem together with the 4^{19} bursting state at $k_8=2.5$, which is confined to the region in phase space where the subcritical Hopf SH_1 and the saddle-node bifurcation SNP_1 occur in the fast subsystem. The dotted line $\dot{p}=0$ denotes the nullcline of Eq. (7); i.e., it indicates in which region of phase space the trajectory (medium solid line) moves to the left ($\dot{p}<0$ below the nullcline) and to the right ($\dot{p}>0$ above the nullcline). Note that the orbit is always confined to the neighborhood of the invariant states of the fast subsystem. At the present value of $k_8=2.5$, the orbit makes four loops close to the cylinderlike manifold before it "jumps" to the linelike manifold where it performs 19 small oscillations. This can be seen in Fig. 7(c), which shows a magnification of the dotted rectangular region in Fig. 7(b). In general, a L^S state wraps L times around the cylinderlike manifold and oscillates S times along the linelike manifold. In Fig. 7(d) a three-dimensional view of the 4^{19} state in the (x,y,p) coordinate system is presented together with a projection onto the x-y plane which again demonstrates the unfolding of the bursting state along the p direction.

1. Sub-Hopf/fold-cycle bursting

In order to clarify how the bifurcations in the fast subsystem lead to the emergence and disappearance of the bursting oscillations, one turn of the trajectory of the 4^{19} MMO is described in detail. We begin to the left of the SNP_1 point in Figs. 7(b) and 7(c) where the linelike quasistationary manifold is the only attractor. Since it is entirely composed of stable stationary states of the fast subsystem (6) which are foci, the trajectory performs damped oscillations along this manifold [Fig. 7(c)]. Subsequent to the subcritical Hopf point SH_1, the foci change stability and, hence, the quasistationary manifold becomes unstable. Accordingly, the amplitude of the oscillations increases again while the trajectory gets more and more attracted by the invariant cylinderlike manifold that consists of stable limit-cycle solutions of the fast subsystem. In the following the trajectory wraps around the cylinderlike manifold while it performs large amplitude oscillations. During that period, the orbit spends some time above and some time below the plane defined by the nullcline equation $\dot{p}=0$ [Fig. 7(b)]. In total, however, there is an effective movement of the trajectory towards lower p values until it passes the saddle-node bifurcation point SNP_1 where it jumps back to the linelike quasistationary manifold to complete one revolution. The reason for the net movement towards lower p values is the slowing down effect that the linelike quasistationary manifold exerts on the part of the trajectory above the nullcline plane where the velocity along the trajectory is much smaller than below the nullcline plane. Thus, in the phase of large amplitude oscillations p decreases except for slow increases during short passages near the linelike manifold.

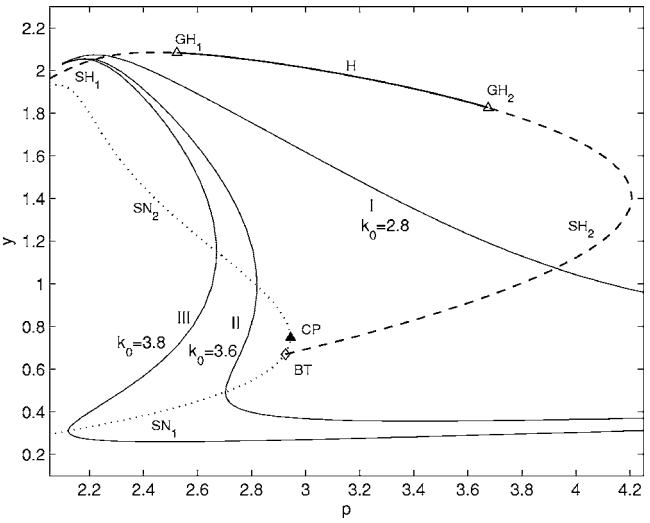

FIG. 8. Overlay of one- and two-parameter bifurcation diagrams for the fast subsystem (6): Curves I, II, and III show how the branch of stationary states of the fast subsystem changes as the flow rate k_0 is increased from 2.8 via 3.6 to 3.8. The codimension-1 bifurcations occurring along curves I, II, and III are found at the intersection points of these curves with the two-parameter continuation curves SH_i and SN_i. Symbols denote SH_i, curves of subcritical Hopf bifurcations (dashed line); H, curve of supercritical Hopf bifurcations (solid line); SN_i, curves of saddle-node bifurcations of fixed points (dotted line); codimension-2 points: GH_i, generalized Hopf bifurcations (open triangle); BT, Bogdanov-Takens (diamond); CP, cusp (solid triangle).

According to the classification of bursting mechanisms given in Ref. [14], the hemin system is a sub-Hopf/fold-cycle burster at $k_0=2.8$ since the large amplitude oscillations terminate by a fold-cycle bifurcation (SNP_1) while the small oscillations disappear via a subcritial Hopf bifurcation (SH_1). As we shall show in the next subsection, there is a transition in the bursting behavior at higher values of the flow rate k_0.

B. Two-parameter continuation in p and k_0

So far we have analyzed the bifurcations in the fast subsystem (6) at one particular value of the external bifurcation parameter, i.e., at $k_0=2.8$. We will now study how the invariant states of the fast subsystem change as k_0 is varied. To this purpose we again proceed in two steps: First, we monitor the deformation of the linelike quasistationary manifold corresponding to the branch of stationary solutions of the fast subsystem. In the second step, we also include the oscillatory states and present a complete two-parameter bifurcation diagram of the fast subsystem using the slow variable p and the flow rate k_0 as parameters.

In Fig. 8 we show how the linelike quasistationary manifold deforms as the flow rate k_0 is increased from the value 2.8 (I) used in the previous section via 3.6 (II) to 3.8 (III). Along these curves, we find certain codimension-1 bifurcations which are connected by curves obtained from a two-parameter continuation using p and k_0 as parameters. For example, the curve I intersects the branches SH_1 and SH_2 (dashed lines) in two points where subcritical Hopf bifurca-

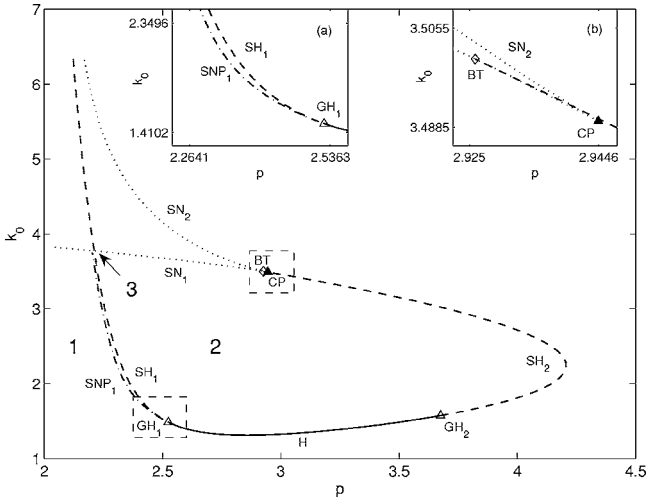

FIG. 9. Two-parameter bifurcation diagram of the fast subsystem (6) using the slow variable p and the flow rate k_0 as parameters. If p sweeps back and forth between region 1 and 2 crossing the SNP_1 curve, the dynamics of the whole system exhibits bursting behavior. In the neighborhood of the intersection point 3 a transition in the bursting mechanism occurs (see text and Fig. 10 for details). Symbols denote SH_i, curves of subcritical Hopf bifurcations (dashed line); H, curve of supercritical Hopf bifurcations (solid line); SN_i, curves of saddle-node bifurcations of fixed points (dotted line); SNP_1, curve of saddle-node bifurcations of periodic orbits (dash-dotted line); codimension-2 points: GH_i, generalized Hopf bifurcations (open triangle); BT, Bogdanov-Takens (diamond); CP, cusp (solid triangle).

tions occur. These Hopf bifurcations are the same as those in Fig. 7(a).

At a higher value of the flow rate ($k_0=3.495$) there is a Bogdanov-Takens (BT) bifurcation occurring in the fast subsystem where the second branch of subcritical Hopf bifurcations SH_2 terminates. As a consequence, the other two branches of stationary states (II and III) still intersect the first subcritical Hopf bifurcation curve SH_1, but no longer SH_2. Instead, the two branches II and III cross the two saddle-node bifurcation curves SN_1 and SN_2 that emerge at CP from a cusp singularity. Note that the location of the first saddle-node bifurcation point SN_1 moves to lower p values as the flow rate k_0 increases. This may lead to interactions of SN_1 with the oscillatory states that are generated in the subcritical Hopf bifurcation SH_1, but which have been omitted in Fig. 8 for clarity.

The complete two-parameter bifurcation structure of the fast subsystem including the oscillatory states is summarized in Fig. 9 where p and k_0 were used as parameters. The bifurcation lines SH_1, SN_1, etc., are the same as those in Fig. 8. In addition, a branch of saddle-node bifurcations of periodic orbits (SNP_1) is shown which bifurcates from the generalized Hopf bifurcation point GH_1 [cf. inset Fig. 9(a)]. This codimension-2 bifurcation point separates two branches of Hopf bifurcations: a supercritical (H) and a subcritical (SH_1) one. The second inset [Fig. 9(b)] shows a magnification of the region close to the cusp bifurcation point CP where the two branches of saddle-node bifurcations originate.

From the two-parameter bifurcation diagram in Fig. 9, one can identify the invariant sets of the fast subsystem at a given value of the slow variable p which, in turn, determine the potential dynamical properties of the system. For example, region 1 corresponds to the upper stationary state at $y\sim 2$, while we find the cylinderlike manifold that is composed of stable limit cycle solutions in region 2. In addition, there is a small bistable region bounded by the two curves SNP_1 and SH_1 where a limit cycle coexists with a stationary state [cf. Fig. 7(c)]. Thus, one can deduce that whenever the slow p dynamics is such that p sweeps back and forth between region 1 and 2 in phase space while crossing the SNP_1 curve, the hemin system exhibits bursting behavior as described in Sec. IV A.

1. Transition in the bursting behavior

The two-parameter bifurcation diagram shown in Fig. 9 can also be used to identify transitions in the bursting behavior of the hemin system. To this purpose, consider the intersection point $(p,k_0)=(2.211,3.773)$ marked as 3. Here, the subcritical Hopf bifurcation SH_1 and the saddle-node bifurcation SN_1 occur at the same value of p in phase space. Thus, in a neighborhood of the intersection point it becomes possible that the (unstable) oscillatory states emanating from the subcritical Hopf bifurcation may interact with the branch of (unstable) states that originate in the saddle-node bifurcation. In order to show that this truly leads to a transition in the bursting behavior of the hemin system, we compare the bifurcation diagrams of the fast subsystem for two neighboring values of the flow rate k_0.

In Fig. 10 the codimension-1 bifurcation diagrams of the fast subsystem are shown for $k_0=3.6$ [Fig. 10(a)] and $k_0=3.8$ [Fig. 10(c)], respectively. Again, the trajectories (calculated for $k_8=2.5$) are superimposed on the bifurcation diagrams. The typical wave form of the oscillations is displayed in the corresponding time series [Figs. 10(b) and 10(d)]. The branches of stationary states (thin lines) in Figs. 10(a) and 10(c) are the same as the curves II and III in Fig. 8, but now they are supplemented by the oscillatory states (bold lines) arising from the subcritical Hopf bifurcation SH_1. At $k_0=3.6$ the cylinderlike manifold is bounded by the saddle-node bifurcation SNP_1 at the left side and the saddle-node homoclinic orbit SNHC at the right side (at $p\sim 2.7$) where the saddle-node bifurcation SN_1 occurs on the large-amplitude-limit cycle.

As the flow rate k_0 increases from 3.6 to 3.8, the saddle-node homoclinic orbit moves together with the two saddle-node bifurcation points SN_1 and SN_2 towards lower p values until the first of them (SN_1) collides with the unstable limit cycle (bold dashed line) at approximately $k_0\sim 3.778$ (not shown), i.e., slightly above the intersection point 3 of Fig. 9. Subsequent to this bifurcation, the saddle-node homoclinic orbit (SNHC) has turned into a saddle homoclinic orbit (SHC) while the saddle-node bifurcation SNP_1 has disappeared [Fig. 10(c)]. Thus, the cylinderlike manifold [Fig. 10(a), bold solid lines] does not appear anymore for $k_0>3.778$ and the fast subsystem becomes bistable. Henceforth, the bursting behavior of the hemin system is of fold/sub-Hopf type since the upper stationary state disappears via the subcritical Hopf bifurcation SH_1 while the lower stationary state undergoes a fold bifurcation at SN_1. A typical tra-

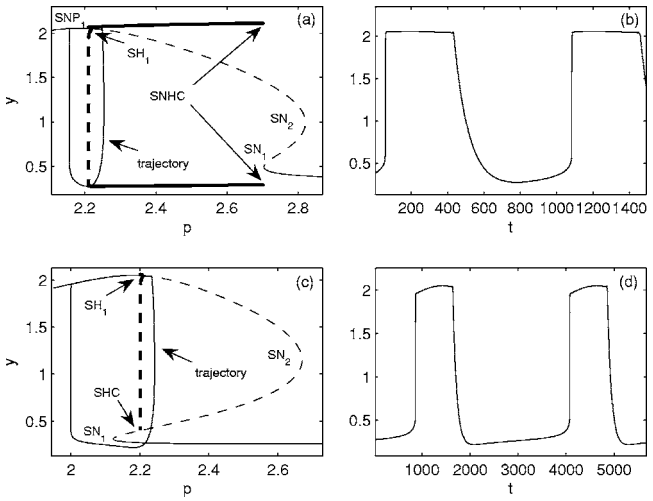

FIG. 10. Transition in the bursting behavior from sub-Hopf/fold-cycle at $k_0=3.6$ (a),(b) to fold/sub-Hopf type at $k_0=3.8$ (c),(d). (a),(c) show codimension-1 bifurcation diagrams of the fast subsystem together with trajectories calculated for $k_8=2.5$ while (b),(d) depict the corresponding time series. As the flow rate k_0 increases, the invariant cylinderlike manifold (formed by stable limit cycles of the fast subsystem) is destroyed as the location of the saddle-node bifurcation SN_1 approaches the unstable limit cycle that is created in the subcritical Hopf bifurcation SH_1 (a). Henceforth, the fast subsystem is bistable (c) and only relaxational oscillations are observed (d). Symbols denote SH_1, subcritical Hopf bifurcation; SNP_1, saddle-node bifurcation of periodic orbit; SN_i, saddle-node bifurcation of fixed points; SHC, saddle homoclinic orbit; SNHC, saddle-node homoclinic orbit. Solid and dashed bold lines denote maxima and minima of a stable and an unstable limit cycle while solid and dashed lines denote stable and unstable fixed points of the fast subsystem.

jectory basically jumps back and forth between the two quasistationary states [Fig. 10(c)], causing the strong relaxational character of the oscillations [Fig. 10(d)].

V. DISCUSSION

The bifurcation structure of the hemin–hydrogen-peroxide–sulfite system was analyzed in detail using a three-dimensional approximation [Eqs. (1) and (4)] which is in very good quantitative agreement with the originally six-dimensional system [25]. A systematic two-parameter continuation in the flow rate k_0 and the hemin decay rate k_8 revealed (cf. Fig. 1) that, depending on the value of the hemin decay rate, simple periodic oscillations either arise from a supercritical Hopf bifurcation or from a sequence of codimension-1 bifurcations starting with a subcritical Hopf bifurcation which is followed by a saddle-node bifurcation of periodic orbits and a Neimark-Sacker bifurcation (inset, Fig. 2).

At higher values of the flow rate k_0, the simple oscillations undergo a transition to mixed-mode or bursting oscillations that occur past a sequence of period-doubling bifurcations (PD in Fig. 1). This suggests that the MMO's in the hemin system cannot be attributed to phase-locked states on a two-torus which is stable in a region close to the branch of subcritical Hopf bifurcations SH_1. In fact, the transition to bursting oscillations involves an entire cascade of period-doubling bifurcations which is accompanied by the formation of a chaotic attractor before the first mixed-mode state is observed at $k_0=2.545$ where 11 large amplitude oscillations alternate with 20 small amplitude oscillations (cf. Figs. 4 and 5).

Next, we described the periodic-chaotic progressions of mixed-mode states that were observed along a one-parameter path taken at $k_8=2.5$ in Fig. 1. They are arranged in periodic windows corresponding to a particular number L of large amplitude oscillations. Within each periodic window, period-adding sequences of L^S states with a different number S of small amplitude oscillations are encountered. Transitions between adjacent states L^S and L^{S+1} occur via narrow chaotic windows where periodic concatenated states of the form $L^S L^{S+1}$ are embedded. Similar bifurcation sequences were also observed by Hauser and Olsen [3] in the PO system and Koper [19] in a three-variable model system.

The observation that mixed-mode states L^S of a gradually decreasing number L of large amplitude oscillations alternate with narrow chaotic windows, together with the fact that a chaotic attractor was formed prior to the observation of the first mixed-mode state, suggests that the bursting oscillations might actually be embedded in a chaotic attractor similar to a scenario reported by Goryachev and colleagues [22].

In that article it is argued that the mixed-mode states are embedded in a horseshoe-type attractor. The bifurcations of the MMO's are described on the basis of a detailed investigation of a suitable Poincaré map from which the transformation of the system's slow manifold into a horseshoe-type attractor was derived as parameters are varied. During the transformation process, Poincaré maps are observed that are very similar to the one we calculated in Fig. 4(c) subsequent to the period-doubling bifurcation. In particular, Goryachev *et al.* also observe a tent map with almost cuspoid tip [cf. Fig. 5(e) in [22]]. For the hemin system, however, it remains an open task to find a Poincaré section that is well defined for the whole parameter range of k_0 values, where the bursting oscillations are stable. Such a Poincaré section would facilitate the establishment of a closer link of the bursting dynamics in the hemin system to the mechanism proposed in [22].

In order to investigate the bursting behavior of the mixed-mode oscillations, we exploited the slow-fast structure of the ODE system (4) and used the slowly evolving variable p as a (quasistatic) bifurcation parameter for the two-dimensional fast subsystem (6). By this analysis, the bursting behavior of the three-dimensional system was classified according to the bifurcations in the fast subsystem leading to the emergence and disappearance of the small amplitude oscillations. Figure 7 shows that at $k_0=2.8$ the system is a sub-Hopf/fold-cycle burster according to the classification given by Izhikevich [14].

A subsequent two-parameter continuation of the fast subsystem in the slow variable p and the flow rate k_0 revealed a transition in the bursting mechanism at $k_0 \sim 3.778$ by which the hemin system becomes a fold/sub-Hopf burster due to a change in the nature of the homoclinic orbit in the fast subsystem [cf. Figs. 10(a) and 10(c)]. At $k_0=3.6$ [Fig. 10(a)], the

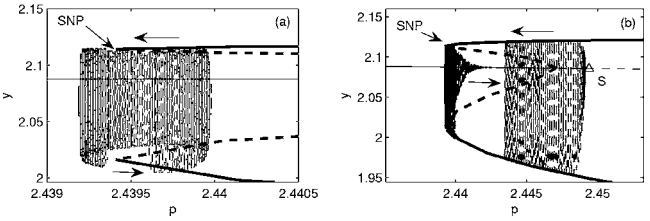

FIG. 11. Slow-fast analysis of behavior in the neighborhood of the Neimark-Sacker bifurcation at $k_0=1.6519$ (cf. Fig. 3): Close to the Neimark-Sacker point at $k_0=1.65189$, the trajectory basically sweeps back and forth the saddle-node bifurcation point SNP of the fast subsystem (a). As the flow rate k_0 decreases to $k_0=1.6518$, the phase flow on the torus changes: The trajectory approaches the stable manifold of the saddle point *S* (open triangle) in damped oscillations as the saddle-node bifurcation point SNP is passed to the left (b). Along the two-dimensional unstable manifold of the saddle point *S*, the trajectory reaches the cylinderlike manifold (bold solid lines) that is composed of stable limit cycle solutions of the fast subsystem. As the trajectory slowly moves to the left, it performs large amplitude oscillations in the vicinity of the cylinderlike manifold until it again passes the saddle-node bifurcation point SNP.

fast subsystem has an orbit that is homoclinic to the nonhyperbolic equilibrium at $p\sim 2.7$ since the saddle-node bifurcation SN_1 occurs on the large amplitude limit cycle. In contrast, at $k_0=3.8$ [Fig. 10(c)], the saddle-node homoclinic orbit SNHC has turned into the saddle homoclinic orbit SHC which involves a hyperbolic equilibrium at $p\sim 2.2$.

The slow-fast analysis also revealed an interesting explanation concerning the origin of quasiperiodic behavior in the hemin system. In Fig. 11 we show the same projections of the phase flow on the torus as in Figs. 3(a) and 3(c), but this time superimposed with the bifurcation diagrams obtained from the slow-fast analysis of the fast subsystem (6). The arrows indicate the direction of the flow on the torus. SNP marks the location where a saddle-node bifurcation of periodic orbits occurs. In addition, there is a subcritical Hopf bifurcation at $p\sim 2.447$ where an unstable (bold dashed lines) limit cycle emerges. Thus, the bifurcation scenario in the fast subsystem is similar to that shown in Fig. 7 where we have analyzed the bursting oscillations at $k_0=2.8$.

Notice how the flow always follows the invariant states of the fast subsystem. For example, at $k_0=1.651\,89$, the trajectory basically sweeps back and forth the saddle-node bifurcation point SNP while it performs large amplitude oscillations in the vicinity of the cylinderlike manifold (bold solid line), thereby creating also quasiperiodic behavior [Fig. 11(a)]. As long as the amplitude of the oscillations along the "inner part" of the cylinderlike manifold is sufficiently large, the trajectory does not "feel" the attractive linelike quasistationary manifold (thin solid line) and, therefore, remains in the neighborhood of the cylinderlike manifold.

However, as the flow rate k_0 is decreased, the phase flow on the torus changes [Fig. 11(b)]: As soon as the saddle-node point SNP is passed to the left, the trajectory gets attracted by the linelike quasistationary manifold. It is the saddle-node point that causes the trajectory to change its direction. Then the orbit returns to the saddle point *S* along its stable manifold which, apparently, is confined to a neighborhood of the linelike quasistationary manifold. Subsequently, the trajectory moves along the two-dimensional unstable manifold of the saddle point *S* to approach the cylinderlike manifold where it performs large amplitude oscillations while slowly moving to the left until the saddle-node point SNP is passed again and the next cycle begins.

The results shown in Fig. 11 suggest that quasiperiodic behavior in the hemin system is due to the coupling of an oscillator in the fast *x*-*y* subsystem (which is represented by the stable-limit-cycle solution) with the slow variable *p*, but on a slow time scale. Indeed, a similar line of argument has been used by Koper [19] to explain the origin of quasiperiodicity in a different system although a slow-fast analysis was not performed to support this statement. However, since tori with a phase flow similar to the one shown in Fig. 11 have been observed in several chemical systems [17–19], it is very likely that they share a common dynamical origin that can be analyzed by a suitable slow-fast analysis.

ACKNOWLEDGMENT

Financial support by the BMBF program CELLECT is gratefully acknowledged.

[1] R. A. Schmitz, K. R. Graziani, and J. L. Hudson, J. Chem. Phys. **67**, 3040 (1977).
[2] J. Maselko and H. L. Swinney, J. Chem. Phys. **85**, 6430 (1986).
[3] M. J. B. Hauser and L. F. Olsen, J. Chem. Soc., Faraday Trans. **92**, 2857 (1996).
[4] C. G. Steinmetz and R. Larter, J. Chem. Phys. **94**, 1388 (1991).
[5] T. Hauck and F. W. Schneider, J. Phys. Chem. **97**, 391 (1993).
[6] X. J. Wang and J. Rinzel, in *The Handbook of Brain Theory and Neural Networks*, edited by M. Arbib (MIT Press, Cambridge, MA, 1995).
[7] L. Glass and M. C. Mackey, *From Clocks to Chaos: The Rhythms of Life* (Princeton University Press, Princeton, NJ, 1988).
[8] L. Brusch, W. Lorenz, M. Or-Guil, M. Br, and U. Kummer, Z. Phys. Chem. (Munich) **216**, 487 (2002).
[9] M. Falcke and D. Malchov, *Understanding Calcium Dynamics* (Springer, Berlin, 2003).
[10] P. M. Dean and E. K. Mathews, J. Physiol. (London) **210**, 255 (1970).
[11] K. Wierschem and R. Bertram, J. Theor. Biol. **228**, 513 (2004).
[12] A. Goldbeter, *Biochemical Oscillations and Cellular Rhythms* (Cambridge University Press, Cambridge, UK, 1996).
[13] J. Rinzel and G. B. Ermentrout, in *Methods in Neuronal Mod-*

eling, edited by C. Koch and I. Segev (MIT Press, Cambridge, MA, 1989).
[14] E. M. Izhikevich, Int. J. Bifurcation Chaos Appl. Sci. Eng. **10**, 1171 (2000).
[15] K. Showalter, R. M. Noyes, and K. Bar-Eli, J. Chem. Phys. **69**, 2514 (1978).
[16] M. J. B. Hauser, L. F. Olsen, T. V. Bronnikova, and W. M. Schaffer, J. Phys. Chem. B **101**, 5075 (1997).
[17] D. Barkley, J. Ringland, and J. S. Turner, J. Chem. Phys. **78**, 3812 (1987).
[18] O. V. Noskov, A. D. Karavaev, V. P. Kazakov, and S. I. Spivak, Mendeleev Commun. 27 (1997).
[19] M. T. M. Koper, Physica D **80**, 72 (1995).
[20] J. Boissonade and P. DeKepper, J. Phys. Chem. **84**, 501 (1980).
[21] J. Ringland, N. Issa, and M. Schell, Phys. Rev. A **41**, 4223 (1990).
[22] A. Goryachev, P. Strizhak, and R. Kapral, J. Chem. Phys. **107**, 2881 (1997).
[23] M. J. B. Hauser, A. Strich, R. Bakos, Zs. Nagy-Ungvárai, and S. C. Müller, Faraday Discuss. **120**, 229 (2001).
[24] M. J. B. Hauser, N. Fricke, U. Storb, and S. C. Müller, Z. Phys. Chem. (Munich) **216**, 375 (2002).
[25] R. Straube, S. C. Müller, and M. J. B. Hauser, Z. Phys. Chem. (Munich) **217**, 1427 (2003).
[26] G. Rabai, K. Kustin, and I. R. Epstein, J. Am. Chem. Soc. **111**, 3870 (1989).
[27] G. Rabai, J. Phys. Chem. A **101**, 7085 (1997).
[28] G. Rabai, A. Kaminaga, and I. Hanazaki, Chem. Commun. (Cambridge) 2181 (1996).
[29] G. Rabai, R. Orban, and I. R. Epstein, J. Phys. Chem. **96**, 5414 (1992).
[30] G. A. Frerichs and R. C. Thompson, J. Phys. Chem. A **102**, 8142 (1998).
[31] G. Rabai and I. Hanazaki, J. Phys. Chem. A **103**, 7268 (1999).
[32] R. Straube, D. Flockerzi, S. C. Müller, and M. J. B. Hauser, J. Phys. Chem. A **109**, 441 (2005).
[33] Y. A. Kuznetsov, *Elements of Applied Bifurcation Theory* (Springer, Heidelberg, 1998).
[34] B. Ermentrout, *Simulating, Analyzing and Animating Dynamical Systems: A Guide to XPPAUT for Researchers and Students* (SIAM, Philadelphia, 2002). See http://www.math.pitt.edu/~bard/xpp/xpp. html
[35] W. H. Press, S. A. Teukolsky, W. T. Vetterling, and B. P. Flannery, *Numerical Recipes in C. The Art of Scientific Computing*, 2nd ed. (Cambridge University Press, Cambridge, UK, 1992).
[36] Y. A. Kuznetsov and V. V. Levitin, CONTENT: A multiplattform environment for analyzing dynamical systems, Dynamical Systems Laboratory, CWI, Amsterdam, 1995–1997, available at ftp.cwi.nl/pub/CONTENT
[37] A. Dhooge, W. Govaerts, and Y. A. Kuznetsov, ACM Trans. Math. Softw. **29**, 141 (2003).